Time-dependent analysis of few-photon coherent control schemes

Shaohao Chen, Agnieszka Jaroń-Becker, and Andreas Becker
JILA and Department of Physics, University of Colorado, Boulder, Colorado 80309-0440, USA
(Received 24 February 2010; published 20 July 2010)

We investigate the coherent control of nonresonant two-photon excitation and $(2+1)$ photon ionization processes from the time-dependent perspective. To this end, we have solved the time-dependent Schrödinger equation for a hydrogen atom interacting with an ultraviolet laser field. Results are obtained for symmetric and antisymmetric phase distributions leading to dark and bright pulses, for which the temporal field distributions consist of many subpulses. For the two-photon excitation process, it is found that at intermediate time between the subpulses, the population in the excited state can exceed the final state population and, in particular, is nonzero for dark pulses. The results for the $(2+1)$ photon ionization closely follow those for the excitation process, which shows that the ionization of the electron proceeds as a resonant process via the excited state in all cases considered.

DOI: 10.1103/PhysRevA.82.013414 PACS number(s): 32.80.Qk, 32.80.Rm

I. INTRODUCTION

In recent years, it has become possible to change phases, amplitudes, and polarization of the different frequency components of a large-bandwidth laser pulse. Because of this development in laser technology, ultrashort laser pulses are nowadays an effective tool to steer quantum processes [1–4]. A variety of control schemes in atoms and molecules have been proposed and demonstrated [5–7]. Some of the applications of coherent control are to control a chemical reaction, to learn about interatomic forces in a molecule, and to create novel stable or metastable molecules [3].

The central idea of coherent control is to either maximize or minimize the probability of a quantum transition between an initial and a final state. Significant progress has been made in the understanding of few-photon coherent control schemes in the perturbative intensity regime. For example, for a two-photon absorption in atoms, induced by an ultrashort laser pulse, one can make use of the interference among various pathways with $\omega_1 + \omega_2 = \omega_0$ between two (bound) states [8]. Here ω_1 and ω_2 are the energies of two photons within the bandwidth of the pulse, and ω_0 is the transition energy between the states. The two-photon absorption probabilities can be tuned to zero (destructive interference) or maximum (constructive interference) by modifying the spectral phase of the pulse. The corresponding pulses are often called dark and bright pulses, respectively. Dark pulses for annihilating the signal of a nonresonant two-photon excitation in an atom have been realized in experiment [4,9]. Extensions of this initial study to form bright [10] as well as dark pulses [11] for resonant two-photon excitation processes have been proposed. Furthermore, a $(2+1)$ photon scheme, in which an intermediate state is reached by a two-photon excitation, to control a three-photon excitation process has been investigated in experiment as well as theory [12–14]. Efforts to analyze quantum control at nonperturbative strong-field intensities [15–17], with shaped femtosecond laser-pulse sequences [18] and for multiphoton ionization [19], have been done recently.

Usually, these few-photon coherent control schemes are analyzed in the frequency domain (e.g., [4]). This provides the opportunity to understand the control over the transition probability in terms of interference effects between different pathways. Since the transitions are driven by an ultrashort laser pulse, it is, however, illustrative to examine the time evolution of these few-photon control schemes as well (e.g., [20–22]). Such an analysis can offer complementary information about the control mechanisms from a direct comparison of the time evolution of the laser field with the instantaneous response of the quantum system.

In this article, we investigate the coherent control of a nonresonant two-photon excitation and a $(2+1)$ photon ionization process from the time-dependent perspective. To this end, we have solved the time-dependent Schrödinger equation for the hydrogen atom interacting with a shaped ultrashort uv laser pulse on a grid. We have chosen the hydrogen atom for this conceptual study since the corresponding numerical solution of the Schrödinger equation can be performed within dipole approximation without further restrictions. The general results of our investigation are, however, applicable for similar transitions in other atoms and at other wavelengths as well.

In the next section, we briefly discuss the control schemes considered in the present study and their applications to the hydrogen atom. We also outline the theoretical method used to obtain the numerical results. In Sec. III A, we present our results on the symmetric and antisymmetric phase control of a two-photon excitation from the ground state of hydrogen to the first excited ($2s$) state. Jointly with these results, we will analyze the $(2+1)$ photon ionization of the H atom via the $2s$ state and discuss similarities in the time evolution of the transition probabilities of both processes. In Sec. III B, we consider control of the same processes by pulses with a π-phase step. The article ends with some concluding remarks.

II. COHERENT CONTROL OF EXCITATION AND IONIZATION IN THE HYDROGEN ATOM

In this section, we first discuss the application of two coherent control schemes to the hydrogen atom, namely, the excitation from the ground state to the first excited state by absorbing two photons and the three photon ionization mediated via the two-photon resonance with the $2s$ state. Then we briefly present the numerical method used to analyze the time evolution of the coherent control processes.

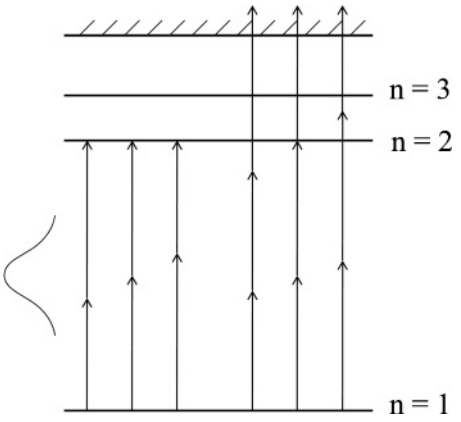

FIG. 1. Control schemes for nonresonant two-photon excitation and $(2+1)$ photon ionization of a hydrogen atom; n denotes the principle quantum number of the eigenstates of the hydrogen atom.

A. Application of control schemes to the H atom

Since numerical solutions of the corresponding Schrödinger equation can be performed on a grid for the hydrogen atom, we have considered this simplest atom for our analysis of the time evolution of few-photon coherent control schemes. In order to study the two-photon excitation and three-photon $(2+1$ photon) ionization process at the same time (cf. Fig. 1), we consider a 243.5 nm uv pulse. The corresponding photon energy of 5.1 eV is half the transition energy (10.2 eV) from the ground state ($1s$) to the first excited state ($2s$) of the hydrogen atom. The probability for a two-photon excitation to the $2s$ state is much larger than that to the $2p$ state because of the selection rule. Three-photon ionization from the ground state ($1s$) to the continuum can be induced as well since the energy of three photons (15.3 eV) is larger than the ionization potential (13.6 eV).

In our calculations, we consider pulses with a spectral bandwidth of 0.4 eV, which corresponds to a pulse duration of 8 fs (full width half maximum) for a transform-limited pulse. With such a bandwidth, there are a lot of coherent pathways for the nonresonant two-photon excitation to the $2s$ state, while an excitation to the next excited state ($3s$) with a transition energy of 12.1 eV will not be induced. On the other hand, the ionization to the continuum can proceed either as a $(2+1)$ photon process via the $2s$ state or as a nonresonant three-photon ionization process.

B. Numerical method

In order to investigate the time evolution of the excitation and ionization processes, we solve the time-dependent Schrödinger equation for the hydrogen atom interacting with a linearly polarized laser pulse on the grid. Because of rotational symmetry over the polarization axis (chosen here as the z axis), the Hamiltonian of the system in dipole approximation and velocity gauge can be written as follows:

$$H(\rho,z,t) = \frac{p_z^2}{2} + \frac{p_\rho^2}{2} + \frac{1}{\sqrt{\rho^2+z^2+a^2}} - \frac{p_z A(t)}{c}, \qquad (1)$$

where z, ρ and p_z, p_ρ are the coordinates and corresponding momenta of the electron parallel and perpendicular to the polarization direction of the laser; $a^2 = 0.001$ is a soft-core Coulomb parameter and $A(t) = -c\int_0^t \widetilde{E}(t)dt$ is the vector potential for the electric field $\widetilde{E}(t)$. The time-dependent Schrödinger equation is solved using the Crank-Nicholson method. The wave functions of the ground, the first, and the second excited states are obtained by imaginary time propagation without the field. The corresponding energies are -13.6 eV, -3.4 eV, and -1.5 eV, which agree well with the exact analytical values. A grid with $N_\rho = 400$ and $N_z = 1000$ points and spacings of $\Delta\rho = \Delta z = 0.1$ au as well as a time step of $\Delta t = 0.02$ au has been used in the calculations. A $\cos^2$ mask function has been applied at the edges of the grid to absorb the outgoing part of the wave packet. Simulations have been performed up to about 10 fs after the end of the pulse.

We have considered a peak intensity of the transform-limited pulse of 4.6×10^{12} W/cm^2, which is in the perturbative intensity regime and can be obtained in experiments. Such a perturbative field strength allows us to evaluate the temporal population of the excited states by projecting the time-dependent wave packet onto the eigenwave functions of unperturbed excited states during the interaction with the pulse. The population of the $2s$ state represents the two-photon excitation probability of present interest. We define the three-photon ionization probability as the absolute square of the outgoing part of the wave packet, absorbed at the edges of the grid. The validity of this method to accumulate the ionization yield via absorption at the boundaries will be discussed later.

III. TIME EVOLUTION OF FEW-PHOTON COHERENT CONTROL PROCESSES

On the basis of second-order time-dependent perturbation theory [23], two useful schemes for controlling nonresonant two-photon excitation processes by modifying the spectral phase of the pulse have been proposed and demonstrated, namely, via a symmetric or antisymmetric phase distribution [4] and by a π-phase step [9]. We consider different phase distributions for both cases and analyze the time evolution of the excitation probability to the $2s$ state and of the ionization probability.

A. Symmetric and antisymmetric phase control

For the case of a symmetric or antisymmetric phase distribution, we write the electric field in the frequency domain as [4]

$$E\left(\frac{\omega_0}{2}+\Omega\right) = E_0\,\mathrm{sech}\left(\frac{1.76\Omega}{\Delta\omega}\right)\exp[i\alpha\cos(\beta\Omega+\phi)], \qquad (2)$$

where $\Delta\omega$ is the bandwidth of the pulse and α, β, and ϕ are the modulation depth, frequency, and phase, respectively. We keep $\beta = 21$ fs as a constant, while α and ϕ are modified to shape the pulse; $\phi = 0$ and $\pi/2$ correspond to symmetric and antisymmetric spectral phase distributions, respectively.

Before we analyze the time evolution, in Figs. 2 and 3, we present the final two-photon excitation probabilities to the $2s$ state and the three-photon ionization probabilities at the end of the pulse as functions of the modulation depth α (Fig. 2) for $\phi = 0$ (circles and solid lines) and $\phi = \pi/2$ (squares and dash-dotted lines), respectively, and of the modulation phase

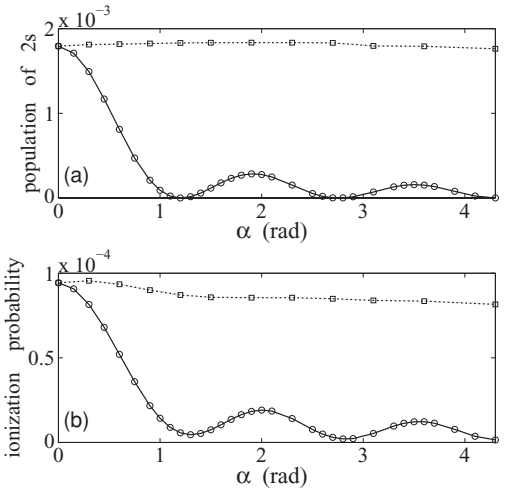

FIG. 2. (a) Population of the $2s$ state and (b) ionization probability as a function of α with $\phi = 0$ (solid line and circles) and $\phi = \pi/2$ (dash-dotted line and squares).

ϕ for $\alpha = 1.2$ (Fig. 3). We note that the general dependence of the results for the two-photon excitation probabilities on the two parameters agrees well with the data measured in the experiment but for the $6S_{1/2}$-$8S_{1/2}$ transition in Cs [4]. This shows that the present numerical method can be applied to analyze the coherent control schemes in the hydrogen atom, while the results will provide insights into such processes more generally.

We see that the theoretical predictions for the three-photon ionization probabilities follow closely the trend of the excitation probabilities in each of the cases considered. For a symmetric spectral phase ($\phi = 0$; Fig. 2, circles and solid lines), both the probabilities vary strongly as α increases and are at minimum (indeed equal to zero for the excitation probability after subtracting the numerical error in the calculations) for certain values of α. For an antisymmetric spectral phase ($\phi = \pi/2$; Fig. 2, squares and dash-dotted lines), the excitation probability maintains almost the same value as the transform-limited pulse as α increases. Fixing $\alpha = 1.2$, both

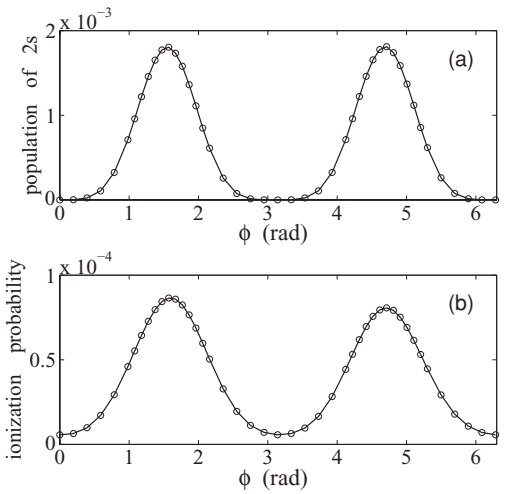

FIG. 3. (a) Population of the $2s$ state and (b) ionization probability as a function of ϕ with $\alpha = 1.2$.

the probabilities can be changed over a large scale from almost zero to the value obtained for a transform-limited pulse for a variation of the phase between 0 and 2π (Fig. 3).

According to perturbation theory, the amplitude of the $(2 + 1)$ photon transition to a higher excited state is proportional to that of the two-photon excitation to a lower excited state [12]. Similar trends of the excitation and ionization probabilities in our calculated results (Figs. 2 and 3) indicate that the $(2 + 1)$ scheme can be applied for ionization to the continuum as well. The maximum ionization probabilities are around 20 times smaller than the excitation probabilities, indicating the low probability to absorb the third photon at these intensities. We note that the ionization probability cannot be turned to zero at the same control parameters as the excitation probability. A similar phenomenon has been seen before for a $(2 + 1)$ photon excitation process [12,13]. In that case, the nonzero probabilities have been explained by nonnegligible contributions of the nonresonant three-photon pathway to the transition amplitude. Subsequently, we will provide a time-dependent analysis for this process, which provides an alternative explanation in the present case.

We now turn to the analysis of the results for the excitation and ionization probabilities as a function of time. The field of the shaped pulse as a function of time $\widetilde{E}(t)$ is obtained by Fourier transform of $E(\omega)$. Variation of the control parameters α and ϕ changes the temporal distribution of the electric field strength and the carrier to envelope phase (CEP). For example, the temporal distribution shows only one pulse for $\alpha = 0$ (transform-limited pulse), while there are many subpulses with different peak field strengths for nonzero α [e.g., cf. Fig. 4(a)]. The field strength $\widetilde{E}_j$ and CEP change between adjacent subpulses j and $j + 1$; that is,

$$\widetilde{E}_{j+1}(t + \Delta t) = c_{j+1,j}\widetilde{E}_j(t)\exp(i\Phi_{j+1,j}), \tag{3}$$

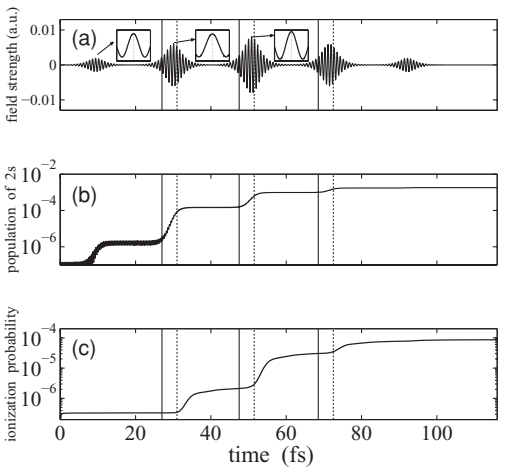

FIG. 4. Comparison of the time evolutions of (a) the electric field strength, (b) the population of the $2s$ state, and (c) the ionization probability for an antisymmetric phase distribution ($\phi = \pi/2$) at $\alpha = 1.2$. Insets of (a) show enlarged views on the central cycles of the first three subpulses shown in the figure. The solid and dashed lines indicate the onsets of increases in the excitation and ionization probability, respectively. Note that there is a time delay of about 4 fs between the onsets.

where $c_{j+1,j}$ denotes the ratio of the field strengths, $\Phi_{j+1,j}$ is the difference in the CEP, and Δt is the time delay between two adjacent subpulses; $c_{j+1,j}$ and Δt depend on the modulation depth α only, while the CEP difference $\Phi_{j+1,j}$ can be tuned by varying the modulation depth α and the spectral phase ϕ.

On the basis of second-order perturbation theory, the two-photon transition amplitude $a_j(t)$ between two bound states induced by the jth pulse is proportional to the square of field strength $\widetilde{E}_j^2(t)$; hence

$$a_{j+1}(t+\Delta t) = c_{j+1,j}^2 a_j(t) \exp(2i\Phi_{j+1,j}). \tag{4}$$

Hence the two-photon excitation probability induced by two adjacent subpulses is given by the absolute square of the coherent superposition of the corresponding amplitudes:

$$|a_{j+1,j}|^2 = \left|\frac{a_j}{\sqrt{2}}\right|^2 \left[1 + c_{j+1,j}^4 + 2c_{j+1,j}^2 \cos(2\Phi_{j+1,j})\right]. \tag{5}$$

There is a predominantly constructive interference for $0 \leqslant \Phi_{j+1,j} < \pi/4$ (with completely constructive interference for $c_{j+1,j} = 1$ and $\Phi_{j+1,j} = 0$) and predominantly destructive interference for $\pi/4 < \Phi_{j+1,j} \leqslant \pi/2$ (with completely destructive interference for $c_{j+1,j} = 1$ and $\Phi_{j+1,j} = \pi/2$). As a function of time, we therefore expect that the excitation probability will steadily increase as long as the interference between the adjacent subpulses is constructive, while the population in the excited state will fluctuate if the interference is destructive.

In Figs. 4 and 5, we present the field strength, the population of the first excited ($2s$) state, and the ionization probability as a function of time for $\alpha = 1.2$. A comparison for an antisymmetric ($\phi = \pi/2$; Fig. 4) and symmetric ($\phi = 0$; Fig. 5) phase distribution is shown. These cases correspond to the maximum (bright pulse) and minimum (dark pulse) final transition probability, respectively (cf. Fig. 3).

For the antisymmetric phase distribution, the CEP difference is equal to zero for adjacent pulses [cf. insets of Fig. 4(a)], indicating a constructive interference of the excitation amplitudes. This is in agreement with the numerical results [Fig. 4(b)], which show that the population in the $2s$ state increases stepwise whenever the atom interacts with one of the subpulses. At the end of the last subpulse, it reaches a value almost equal to that induced by the transform-limited pulse. The ionization probability follows the trend of the excitation probability [Fig. 4(c)]. Note that there is a time delay between the onset of the increases in the curve of the ionization probability (indicated by dashed lines) as compared to those in the curve for the excitation probability (indicated by solid lines). The time delay is due to the fact that we define ionization of the atom via the absorption of the wave packet at the boundaries of the grid. Considering the kinetic energy of the ionizing electron (15.3–13.6 eV = 6.25×10^{-2} au) and the extension of the grid along the polarization direction (50 au), a rough classical estimate yields that the ionizing wave packet needs about 4 fs to propagate from the center of the grid (i.e., the nucleus) to the boundaries. This estimation agrees well with the time delay seen in the results. From the results for the time evolution of the ionization probability [Fig. 4(c)], we see that it depends on the population in the $2s$ state as well as the field strength. This is in agreement with the expectation that at these field strengths, the ionization of the electron proceeds as a $(2+1)$ photon transition via the $2s$ state. There is no signature for a contribution of the nonresonant three-photon transition to the continuum seen in the data.

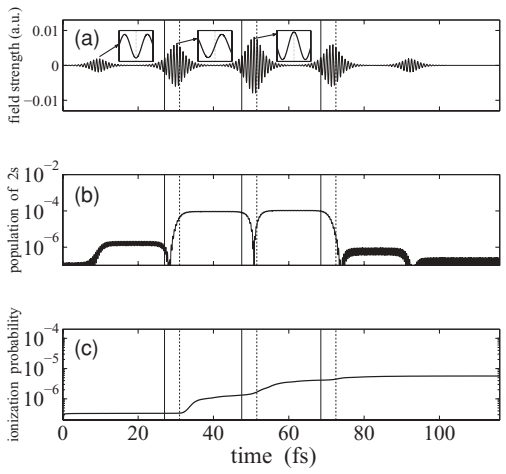

FIG. 5. Same as Fig. 4, but for a symmetric spectral phase distribution ($\phi = 0$) at $\alpha = 1.2$. The dashed lines indicate the onsets in the ionization probability, while the solid lines indicate the corresponding times, taking into account the 4 fs time delay between detection of excitation and ionization in the present calculations.

In the case of the symmetric phase distribution, the difference between the CEPs of adjacent subpulses is equal to $\pi/2$ [cf. insets of Fig. 5(a)]. Therefore the two-photon excitation amplitudes induced by adjacent subpulses interfere destructively. This trend is reflected in the time-dependent population of the $2s$ state [Fig. 5(b)]. It rises during the first subpulse and then decreases to zero during the first part of the following subpulses, while it rises again over the second part of the subpulses. Finally, it drops to zero at the end of the last subpulse. Since the field strengths in the adjacent pulses differ ($c_{j+1,j} \neq 1$), there is no complete destructive interference between the amplitudes, and the $2s$ population is nonzero at intermediate time between the subpulses.

From the results for the time evolution of the ionization probability [Fig. 5(c)], we see that each onset of the increases corresponds to instants (considering the time delay discussed earlier) when the electric field is rather weak but the excitation probability is high. We therefore conclude that the ionization primarily depends on the population in the $2s$ state. This is in agreement with our preceding interpretation that at these field strengths, the ionization of the electron proceeds via a $(2+1)$ photon process. Note that the final ionization probability is nonzero, which is due to the nonzero population of the excited states at intermediate time.

As discussed earlier, we identify the ionization process as a $(2+1)$ process, that is, a single-photon process from the excited $2s$ state, by relating the onsets in the ionization probability to those time instants at which the excitation probability in the $2s$ state is high. In case of a nonresonant three-photon ionization, which is a nonlinear process, the rises in the ionization probability should clearly correlate to the maxima in the field strength. In particular, for the so-called dark pulse, this is not the case, and we therefore rule out any

TABLE I. Comparison of the ionization probabilities, calculated via absorption at the boundaries (first line) and via the projection method [Eq. (6), second line], at an intermediate time after two adjacent pulses. Parameters are the same as in Figs. 4 and 5.

Grid size	P_{ion} (Fig. 4)	P_{ion} (Fig. 5)
400×1000	2.33×10^{-6}	1.45×10^{-6}
2000×6000	2.43×10^{-6}	1.46×10^{-6}

(significant) contribution of the nonresonant process in the present cases.

We further note that in the case of a $(2+1)$ photon ionization process, we do not expect a destructive interference effect between the ionizing wave packets created by adjacent subpulses. In order to test our expectation, we have repeated some of the calculations on a larger grid ($N_\rho = 2000$ and $N_z = 6000$ points), which enabled us to keep the whole wave function on the grid well after the second pulse (without any absorption at the boundaries) for the results presented in Figs. 4 and 5. At an intermediate time t_{int} after the second subpulse, we calculated the ionization probability by

$$P_{\text{ion}}(t_{\text{int}}) = \int dz\, d\rho\rho \Big| \Psi(\rho,z,t_{\text{int}}) - \sum_{nl} < \phi_{nl} | \Psi(\rho,z,t_{\text{int}}) > \phi_{nl} \Big|^2, \qquad (6)$$

where $\Psi(\rho,z,t_{\text{int}})$ is the time-dependent wave function at t_{int} and ϕ_{nl} is the (n,l)th eigenstate of hydrogen atom. In Table I, the results of these calculations are compared with those obtained on the small grid via the absorption of the wave packets at the boundaries for the parameters in Figs. 4 and 5. As expected, the results agree well with each other, which implies that interference effects between adjacent wave packets do not play a role and justifies the definition of the ionization yields via absorption at the boundaries in the present cases.

We also considered a symmetric phase distribution ($\phi = 0$) but $\alpha = 1.9$ (Fig. 6), at which a local maximum in the excitation probability as a function of α is found (cf. Fig. 2). The final excitation probability is, however, smaller than that for the transform-limited pulse. The CEP differences indicate

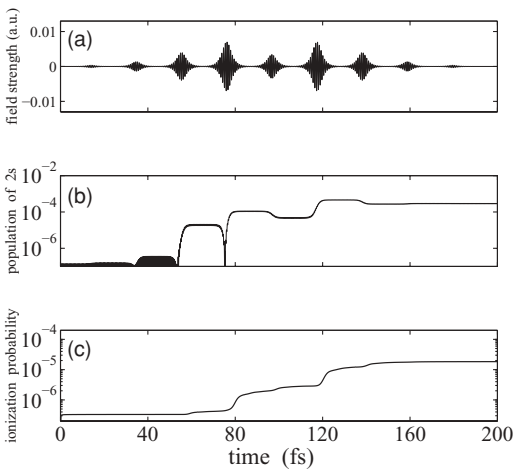

FIG. 6. Same as Fig. 4, but for $\phi = 0$ and $\alpha = 1.9$.

in this case a partial destructive or constructive interference between adjacent subpulses. Hence the time evolution of the population in the $2s$ state shows a more complex pattern than in the previous cases. Interestingly, at certain intermediate times, the probability of finding the electron in the excited state is larger than the final transition probability. On the other hand, the temporal evolution of the ionization probability can be explained as before; that is, the larger the population in the $2s$ state and the larger the field strength, the stronger is the increase in the ionization probability.

B. Step control in the π phase

For the second case, namely, a phase distribution with a π-phase step, the electric field strength in the frequency domain can be written as [9]

$$E\left(\frac{\omega_0}{2}+\Omega\right) = E_0 \text{sech}\left(\frac{1.76\Omega}{\Delta\omega}\right) \exp\left[i\,\text{sgn}(\Omega-\delta)\frac{\pi}{2}\right], \qquad (7)$$

where $\text{sgn}(x) = \pm 1$ according to the sign of x and δ is the phase step position, which is the control parameter to shape the pulse. As a function of time, the field strength can be written as

$$\widetilde{E}\left(\frac{T}{2}+t\right) = \widetilde{E}\left(\frac{T}{2}-t\right)\exp(i\,\Phi), \qquad (8)$$

where T is the full pulse duration and Φ is the CEP difference between the two parts of the pulse. The two-photon excitation probability induced by the two parts will therefore constructively or destructively interfere, depending on the value of Φ.

The numerical results for the two-photon excitation probability in the hydrogen atom as a function of the π-phase step position [Fig. 7(a)] agree well with the experimental data and theoretical predictions found in Cs [9]. There is a minimum at $\delta = \pm 0.31$ (equal to zero after subtracting the numerical error), corresponding to a dark pulse. As in the case of the symmetric and antisymmetric phase control, the dependence of the three-photon ionization probability on the phase step

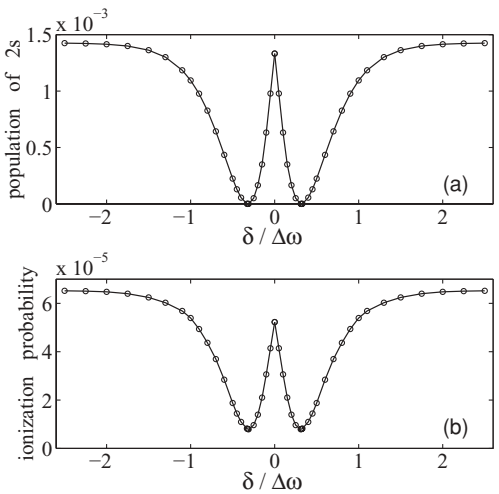

FIG. 7. (a) Population of the $2s$ state and (b) ionization probability as a function of π-phase step position δ.

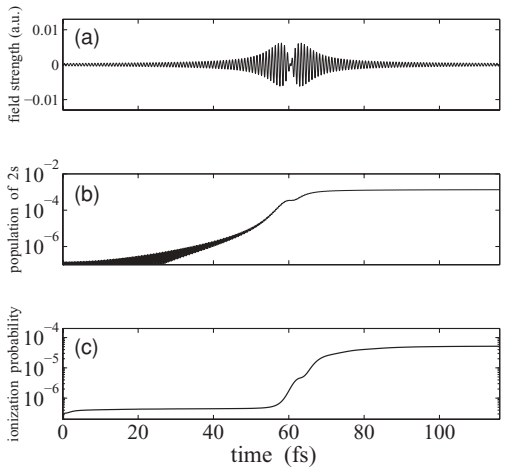

FIG. 8. Comparison of the time evolutions of (a) the electric field strength, (b) the population of the $2s$ state, and (c) the ionization probability at the local maximum ($\delta = 0$).

position [Fig. 7(b)] is very similar to that of the two-photon excitation probability.

The results for the time evolution of the population in the $2s$ excited state and of the ionization probability confirm the conclusions drawn earlier. For $\delta = 0$ (Fig. 8), the CEP difference between the two parts of the electric field [Fig. 8(a)] is zero; hence the interference is constructive and the two-photon excitation probability is steadily increasing [Fig. 8(b)]. The ionization probability [Fig. 8(c)] follows the trend and shows, as expected, strong increases if the instantaneous excitation probability is high and the field strength is large. In contrast, for $\delta = 0.31$ (Fig. 9), the CEP difference between the two parts of the electric field is $\pi/2$ [Fig. 9(a)] and the interference is destructive. Therefore the excitation probability [Fig. 9(b)] increases during the first part and decreases to zero over the second part of the pulse. The ionization probability [Fig. 9(c)] increases over the first part of the pulse and remains almost a constant over the second part, as the excitation probability decreases. These results suggest as well that the nonzero ionization probability is because of an intermediate population of the $2s$ state rather than a contribution of the nonresonant

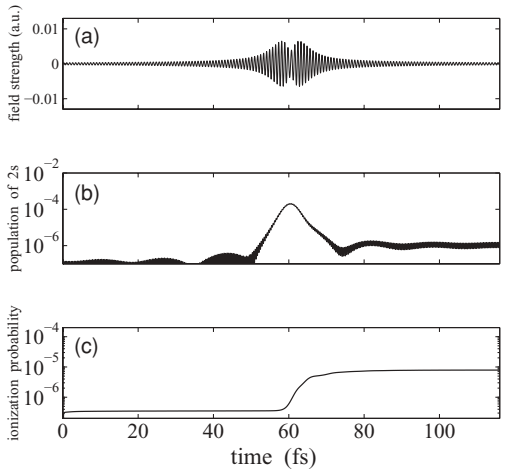

FIG. 9. Same as Fig. 8, but at the minimum ($\delta = 0.31$).

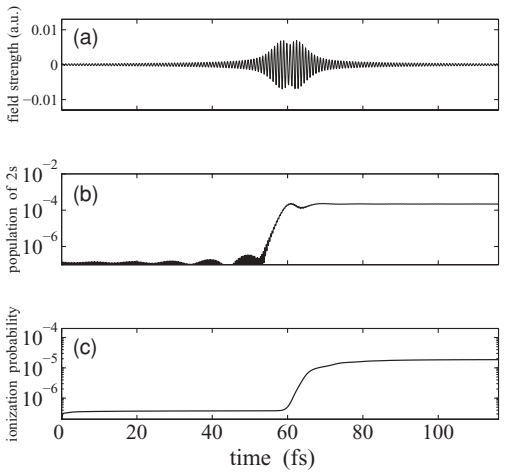

FIG. 10. Same as Fig. 8, but at $\delta = 0.5$.

three-photon pathway. Finally, we present in Fig. 10 the time evolutions for an intermediate case, namely, $\delta = 0.5$. The CEP difference between the two parts of the electric field is between zero and $\pi/2$, indicating partial destructive or partial constructive interference. As in the previous section, the time-dependent population in the $2s$ state [Fig. 10(b)] is fluctuating over the second part of the pulse with intermediate probabilities even slightly larger than the final probabilities. Correspondingly, the ionization probability shows a stepwise increase.

IV. CONCLUDING REMARKS

To summarize, we have studied few-photon coherent control schemes from the time-dependent perspective. To this end, we have solved the time-dependent Schrödinger equation for the hydrogen atom interacting with shaped linearly polarized laser pulses. The probabilities for nonresonant two-photon transition to the $2s$ state and $(2+1)$ photon ionization to the continuum have been evaluated as a function of time. For different phase distributions, the results for the excitation probabilities are found to agree well with previously published experimental data (taken in Cs). It is found that the time-dependent analysis offers complementary information about the control mechanism as compared to studies in the frequency domain. The maxima (minima) in the final excitation probabilities are because of constructive (destructive) interferences between the amplitudes induced by different subpulses. At intermediate time, the population in the excited state is found to be nonzero, even for dark pulses, and may exceed the final transition probability. Our results for the ionization probabilities are found to depend on the degree of excitation in the $2s$ state and the field strengths. This indicates that at the present field parameters, the ionization proceeds via a resonant (via the $2s$ state) rather than a nonresonant process.

ACKNOWLEDGMENT

This work was supported by NSF and DOE.

[1] S. A. Rice, Science **258**, 412 (1992).
[2] W. S. Warren, H. Rabitz, and M. Dahleh, Science **259**, 1581 (1993).
[3] H. Rabitz, R. Vivie-Riedle, M. Motzkus, and K. Kompa, Science **288**, 824 (2000).
[4] D. Meshulach and Y. Silberberg, Nature **396**, 239 (1998).
[5] S. A. Rice and M. Zhao, *Optimal Control of Molecular Dynamics* (Wiley-Interscience, New York, 2000).
[6] M. Shapiro and P. Brumer, *Principles of the Quantum Control of Molecular Processes* (Wiley, Hoboken, 2003).
[7] D. J. Tannor, *Introduction to Quantum Mechanics: A Time-Dependent Perspective* (University Science Books, Sansilito, 2006).
[8] Hartree atomic units ($e = m_e = \hbar = 1$) are used unless mentioned otherwise.
[9] D. Meshulach and Y. Silberberg, Phys. Rev. A **60**, 1287 (1999).
[10] N. Dudovich, B. Dayan, S. M. Gallagher Faeder, and Y. Silberberg, Phys. Rev. Lett. **86**, 47 (2001).
[11] P. Panek and A. Becker, Phys. Rev. A **74**, 023408 (2006).
[12] A. Gandman, L. Chuntonov, L. Rybak, and Z. Amitay, Phys. Rev. A **75**, 031401(R) (2007).
[13] A. Gandman, L. Chuntonov, L. Rybak, and Z. Amitay, Phys. Rev. A **76**, 053419 (2007).
[14] Z. Amitay, A. Gandman, L. Chuntonov, and L. Rybak, Phys. Rev. Lett. **100**, 193002 (2008).
[15] N. Dudovich, T. Polack, A. Peer, and Y. Silberberg, Phys. Rev. Lett. **94**, 083002 (2005).
[16] L. Chuntonov, L. Rybak, A. Gandman, and Z. Amitay, Phys. Rev. A **77**, 021403 (2008).
[17] H. Suchowski, A. Natan, B. D. Bruner, and Y. Silberberg, J. Phys. B **41**, 074008 (2008).
[18] A. Präkelt, M. Wollenhaupt, C. Sarpe-Tudoran, and T. Baumert, Phys. Rev. A **70**, 063407 (2004).
[19] T. Bayer, M. Wollenhaupt, C. Sarpe-Tudoran, and T. Baumert, Phys. Rev. Lett. **102**, 023004 (2009).
[20] M. Wollenhaupt, A. Präkelt, C. Sarpe-Tudoran, D. Liese, T. Bayer, and T. Baumert, Phys. Rev. A **73**, 063409 (2006).
[21] M. V. Korolkov and K.-M. Weitzel, Chem. Phys. **338**, 277 (2007).
[22] T. Bayer, M. Wollenhaupt, and T. Baumert, J. Phys. B **41**, 074007 (2008).
[23] F. H. M. Faisal, *Theory of Multiphoton Processes* (Plenum, New York, 1987), chap. 2.